The Astrophysical Journal, 813:96 (11pp), 2015 November 10 doi:10.1088/0004-637X/813/2/96

QUANTUM CALCULATION OF INELASTIC CO COLLISIONS WITH H. III. RATE COEFFICIENTS FOR RO-VIBRATIONAL TRANSITIONS

L. Song[1], N. Balakrishnan[2], K. M. Walker[3], P. C. Stancil[3], W. F. Thi[4], I. Kamp[5], A. van der Avoird[1], and G. C. Groenenboom[1]
[1] Theoretical Chemistry, Institute for Molecules and Materials, Radboud University, Heyendaalseweg 135, 6525 AJ Nijmegen, The Netherlands
[2] Department of Chemistry, University of Nevada, Las Vegas, NV 89154, USA
[3] Department of Physics and Astronomy and Center for Simulational Physics, The University of Georgia, Athens, GA 30602, USA
[4] Max Planck Institute for Extraterrestrial Physics, Garching, Germany
[5] Kapteyn Astronomical Institute, PO Box 800, 9700 AV Groningen, The Netherlands
Received 2015 July 20; accepted 2015 September 4; published 2015 November 3

ABSTRACT

We present calculated rate coefficients for ro-vibrational transitions of CO in collisions with H atoms for a gas temperature range of $10\,\mathrm{K} \leqslant T \leqslant 3000\,\mathrm{K}$, based on the recent three-dimensional ab initio H–CO interaction potential of Song et al. Rate coefficients for ro-vibrational $v = 1, j = 0$–$30 \rightarrow v' = 0, j'$ transitions were obtained from scattering cross sections previously computed with the close-coupling (CC) method by Song et al. Combining these with the rate coefficients for vibrational $v = 1$–$5 \rightarrow v' < v$ quenching obtained with the infinite-order sudden approximation, we propose a new extrapolation scheme that yields the rate coefficients for ro-vibrational $v = 2$–$5, j = 0$–$30 \rightarrow v', j'$ de-excitation. Cross sections and rate coefficients for ro-vibrational $v = 2, j = 0$–$30 \rightarrow v' = 1, j'$ transitions calculated with the CC method confirm the effectiveness of this extrapolation scheme. Our calculated and extrapolated rates are very different from those that have been adopted in the modeling of many astrophysical environments. The current work provides the most comprehensive and accurate set of ro-vibrational de-excitation rate coefficients for the astrophysical modeling of the H–CO collision system. The application of the previously available and new data sets in astrophysical slab models shows that the line fluxes typically change by 20%–70% in high temperature environments (800 K) with an H/H_2 ratio of 1; larger changes occur for lower temperatures.

Key words: astronomical databases: miscellaneous – ISM: molecules – molecular data – molecular processes – photon-dominated region (PDR) – protoplanetary disks

Supporting material: machine-readable tables

1. INTRODUCTION

As the second most abundant molecule in the universe, carbon monoxide (CO) is commonly detected in a variety of astrophysical environments. As early as the 1970s, the infrared ro-vibrational bands of CO were observed in late-type stars (Thompson et al. 1969; Johnson & Méndez 1970; Johnson et al. 1972). Later, Scoville et al. (1980) and Ayres (1986) detected CO ro-vibrational lines in the spectra of young stellar objects and the Sun. In a sample of nine infrared sources identified by Mitchell et al. (1990), eight sources show evidence of a hot gas component with temperatures of 120–1010 K and CO ro-vibrational emission. Recently, $\Delta v = 1$ ro-vibrational transitions of CO near 4.7 μm have been observed in star-forming regions, protoplanetary disks, and external galaxies using high-resolution spectrometers (González-Alfonso et al. 2002; Najita et al. 2003; Rettig et al. 2004; Carmona et al. 2005; Salyk et al. 2007; Pontoppidan et al. 2008; Brittain et al. 2009; van der Plas et al. 2009; Goto et al. 2011; Brown et al. 2013; Bertelsen et al. 2014). Analysis of these CO spectral lines provides the physical conditions and chemical composition of the interstellar gas, in particular the kinetic temperature, column density, volume density, and molecular abundances. Many of the analyses assumed that the CO ro-vibrational emission is based on local thermodynamical equilibrium (LTE) populations, which, however, applies only in high-density regions where collisions dominate the excitations. Non-LTE modeling is necessary when infrared and UV fluorescent excitation and radiative de-excitation compete with molecular collisions (van der Tak 2011), and it is required for a detailed understanding of the CO ro-vibrational lines in terms of spatial location and efficiency of the IR/UV fluorescence (Thi et al. 2013). The non-LTE analysis requires accurate collision rate coefficients of CO with its main collision partners, H, H_2, He, and electrons, as input. The lack, or limited reliability, of such rate coefficient data hinders non-LTE modeling of molecular spectra for many astrophysical environments. In particular, rate coefficients for the H–CO system are known to be highly uncertain (Shepler et al. 2007) and difficult to calculate due to the existence of a chemical bond between H and CO. The appearance of a deep well and a dissociation barrier in the H–CO potential make it substantially more difficult to compute converged scattering cross sections than for typical van der Waals systems such as He–CO and H_2–CO. In addition, it was shown in Walker et al. (2014) that standard approaches for scaling He–CO rate coefficients to obtain values for H_2–CO or, especially, H–CO are not valid.

For pure rotational transitions, rate coefficients of H–CO were first given by Chu & Dalgarno (1975) about four decades ago for CO excitation from $j = 0$–4 to $j' = 1$–5 at temperatures of $T = 5$–$150\,\mathrm{K}$. One year later, Green & Thaddeus (1976) reported their values for transitions from initial states with $j = 0$–7 at temperatures of $T = 5$–$100\,\mathrm{K}$. Rate coefficients for pure rotational transitions up to $j = 7$ for a broad range of gas temperatures $T = 5$–$3000\,\mathrm{K}$, were calculated by Balakrishnan et al. (2002). Compared with the earlier values of Green & Thaddeus (1976), their results

differed by a factor of 30 for rate coefficients at temperatures below 100 K. More recently, Shepler et al. (2007) performed scattering calculations with two new ab initio potential energy surfaces and suggested that the pure rotational rate coefficients obtained by Balakrishnan et al. (2002) were incorrect, due to the fact that the WKS interaction potential (Keller et al. 1996) they used for H–CO was inaccurate in its long range part. In a recent paper, Yang et al. (2013) calculated the rotational quenching rate coefficients of low-lying ($j = 1-5$) rotational CO levels for temperatures ranging from 1 to 3000 K. They found pure rotational quenching rate coefficients similar to the values of Green & Thaddeus (1976), which confirms the inaccuracy of results obtained using the WKS potential (Balakrishnan et al. 2002). Very recently, Walker et al. (2015) performed calculations of the pure rotational quenching rates for initial states up to $j = 45$ at a temperature range of $T = 1$–3000 K based on the new three-dimensional (3D) H–CO potential of Song et al. (2013).

For vibrational rate coefficients the situation is still unsatisfactory, however. Experimental values are available only for the rotationally unresolved $v = 1 \rightarrow 0$ transition. The most reliable results were measured by Glass & Kironde (1982) using a discharge-flow shock tube at temperatures between 840 and 2680 K. Other experimental values reported by von Rosenberg et al. (1971) and Kozlov et al. (2000) are based on estimates of the efficiency of H atoms in vibrational relaxation of CO derived from data involving other gases. Quantum scattering calculations of rate coefficients for transitions between vibrational levels up to $v = 4$ were performed by Balakrishnan et al. (2002) with the infinite order sudden (IOS) approximation at temperatures ranging from 100 to 3000 K. Their computed results agreed with the experimental data measured by Glass & Kironde (1982) in the high-temperature range. Vibrational rate coefficients below 100 K were not available, however. Rate coefficients for ro-vibrational transitions were even less complete. Yang et al. (2005) presented quenching rate coefficients for initial states $v = 1$, $j = 0$, 1, 2 to $v = 0$ at a temperature range of $T = 10^{-5}$–300 K. They performed close-coupling (CC) calculations, but their channel basis may have been too small to ensure convergence and they adopted the WKS potential (Keller et al. 1996), known to be inaccurate in the long range. Both factors may lead to uncertainties in the ro-vibrational rate coefficients and the lack of a comprehensive set of H–CO ro-vibrational rate coefficients obliged astronomers to use scaling laws to extrapolate the data (e.g., Thi et al. 2013).

Recently, Thi et al. (2013) modeled CO ro-vibrational emission from Herbig Ae discs using the H–CO rate coefficients calculated by Balakrishnan et al. (2002). They extrapolated the pure rotational de-excitation rate coefficients to initial states with $j > 7$ and vibrational transition rate coefficients to temperatures below 100 K. Assuming complete decoupling of rotational and vibrational motion, they estimated the state-to-state ro-vibrational rate coefficients from the corresponding rates for pure rotational transitions in the ground vibrational level. This method was described in detail and applied to the H_2O–H_2 system by Faure & Josselin (2008). However, extrapolations based on only a few calculated rate coefficients may cause large errors in the deduced rates. Moreover, the above mentioned inaccuracy of the pure rotational rate coefficients derived from the WKS potential (Balakrishnan et al. 2002) will introduce an additional error. In the present paper, we report explicitly calculated state-to-state ro-vibrational de-excitation rate coefficients for $\Delta v = -1$ transitions in H–CO for initial states with $v = 1$ and 2 and j values up to 30 for temperatures ranging from 10 to 3000 K. A new extrapolation method is devised and applied to obtain state-to-state ro-vibrational de-excitation rate coefficients for initial states with v up to 5. A LAMDA-type file (Schöier et al. 2005) is provided with ro-vibrational de-excitation rate coefficients of H–CO for $v = 1$–5, $j = 0$–30 $\rightarrow v', j'$ transitions at temperatures of $T = 10$–3000 K.

2. THEORY

2.1. Equations for Rate Coefficients

The CC calculations were performed using our scattering code described by Song et al. (2015), while the IOS calculations were carried out with the non-reactive scattering program MOLSCAT (Hutson & Green 1994). The scattering methods used to obtain cross sections are reported in detail in our previous paper (Song et al. 2015). Rate coefficients for specific ro-vibrational transitions were calculated by averaging the corresponding cross sections over a Maxwell–Boltzmann distribution of translational energies of the colliding particles,

$$r(T) = \left(\frac{8k_{\rm B}T}{\pi\mu}\right)^{\frac{1}{2}} \frac{1}{(k_{\rm B}T)^2} \int_0^\infty \sigma(E_k) \exp\left(-\frac{E_k}{k_{\rm B}T}\right) E_k dE_k, \quad (1)$$

where μ is the reduced mass of H–CO, $k_{\rm B}$ is the Boltzmann constant and T is the gas temperature. Cross sections were calculated over an energy range from 0.1 to 15,000 $\rm cm^{-1}$, see Song et al. (2015). The integral over collision energies was computed numerically with the trapezoidal rule after cubic spline interpolation of the cross sections on a logarithmic energy scale. The cross section $\sigma(E_k)$ as a function of the collision energy E_k can be the state-to-state ro-vibrational cross section $\sigma_{v,j\rightarrow v',j'}(E_k)$, the total vibrational quenching cross section $\sigma_{v,j\rightarrow v'}(E_k)$ for the transitions from an initial v, j state to a final v' state, or the vibrational transition cross section $\sigma_{v\rightarrow v'}(E_k)$. The quantum numbers v and j refer to the vibration and rotation in the initial state, while v' and j' refer to the final state. The rate coefficients for the reverse transitions can be obtained by detailed balance

$$r_{v',j'\rightarrow v,j}(T) = \frac{2j+1}{2j'+1} \exp\left(\frac{\epsilon_{v',j'} - \epsilon_{v,j}}{k_{\rm B}T}\right) r_{v,j\rightarrow v',j'}(T), \quad (2)$$

where $\epsilon_{v,j}$ and $\epsilon_{v',j'}$ are the energies of the ro-vibrational levels. The state-to-state ro-vibrational cross sections $\sigma^{\rm CC}_{v,j\rightarrow v',j'}(E_k)$ are obtained from full CC calculations; the corresponding rate coefficients can be calculated from Equation (1). By summation of the state-to-state ro-vibrational cross sections over all final j' levels in the v' state, we obtain the total vibrational quenching cross section from a specific ro-vibrational initial state v, j to final state v'

$$\sigma^{\rm CC}_{v,j\rightarrow v'}(E_k) = \sum_{j'} \sigma^{\rm CC}_{v,j\rightarrow v',j'}(E_k). \quad (3)$$

The corresponding rate coefficients are denoted by $r^{\rm CC}_{v,j\rightarrow v'}(T)$. Averaging the rate coefficients $r^{\rm CC}_{v,j\rightarrow v'}(T)$ over a thermal

Table 1

Rate Coefficients from CC Calculations for Ro-vibrational $v = 1, j = 0–30 \rightarrow v' = 0, j'$ Transitions in the Temperature Range of 10 K $\leqslant T \leqslant$ 3000 K (in Units of $cm^3\ s^{-1}$ with the Exponent Denoting Powers of 10)

		T (K)																		
j	j'	10	20	30	40	50	60	70	80	90	100	200	300	500	700	1000	1500	2000	2500	3000
0	0	1.949e-17	1.600e-17	1.585e-17	1.733e-17	2.019e-17	2.449e-17	3.032e-17	3.770e-17	4.674e-17	5.777e-17	8.020e-16	6.025e-15	4.334e-14	1.068e-13	2.096e-13	3.622e-13	4.999e-13	6.316e-13	7.573e-13
0	1	2.427e-17	1.627e-17	1.346e-17	1.281e-17	1.388e-17	1.679e-17	2.172e-17	2.881e-17	3.840e-17	5.135e-17	1.440e-15	1.111e-14	7.466e-14	1.793e-13	3.488e-13	5.965e-13	8.046e-13	9.865e-13	1.148e-12
0	2	2.768e-17	1.751e-17	1.338e-17	1.170e-17	1.152e-17	1.267e-17	1.514e-17	1.900e-17	2.455e-17	3.265e-17	1.297e-15	9.571e-15	5.504e-14	1.260e-13	2.465e-13	4.330e-13	5.900e-13	7.258e-13	8.462e-13

(This table is available in its entirety in machine-readable form.)

population of initial j states yields the vibrational transition rate coefficient based on the CC approach

$$r^{\rm CC}_{v\rightarrow v'}(T) = \frac{\sum_j g_j \exp\left(-\frac{\epsilon_{v,j}}{k_{\rm B}T}\right) r^{\rm CC}_{v,j\rightarrow v'}(T)}{\sum_j g_j \exp\left(-\frac{\epsilon_{v,j}}{k_{\rm B}T}\right)}, \quad (4)$$

where $g_j = 2j + 1$ is the degeneracy of the rotational level j.

The vibrational transition cross sections $\sigma^{\rm IOS}_{v\rightarrow v'}(E_k)$ are obtained directly from scattering calculations in the IOS approximation. The corresponding rate coefficients can again be calculated from Equation (1).

2.2. Extrapolation Method

If we wish to calculate all ro-vibrational rate coefficients of interest for astrophysical modeling, the full CC method is prohibitively expensive. The incompleteness of the available ro-vibrational rate coefficients forced astronomers to use extrapolated data, commonly based on a complete decoupling of vibration and rotation (Faure & Josselin 2008; Thi et al. 2013; Bruderer et al. 2015). Here, we introduce a new extrapolation method for state-to-state ro-vibrational rate coefficients in which we assume the coupling in $v, j \rightarrow v', j'$ transitions with $v' < v$ to be the same as in the $v = 1, j \rightarrow v' = 0, j'$ transition. Then, the state-to-state ro-vibrational rates are related to the corresponding rates for the $v = 1, j \rightarrow v' = 0, j'$ transitions as follows

$$r_{v,j\rightarrow v',j'}(T) = P_{vv'}(T) r_{1,j\rightarrow 0,j'}(T), \quad (5)$$

where the factor $P_{vv'}(T)$ is defined as

$$P_{vv'}(T) = \frac{r_{v\rightarrow v'}(T) \sum_j g_j \exp\left(-\frac{\epsilon_{v,j}}{k_{\rm B}T}\right)}{\sum_j \left[g_j \exp\left(-\frac{\epsilon_{v,j}}{k_{\rm B}T}\right) \sum_{j'} r_{1,j\rightarrow 0,j'}(T) \right]} = \frac{r_{v\rightarrow v'}(T)}{r_{1\rightarrow 0}(T)}. \quad (6)$$

The difference with the extrapolation method used by Thi et al. (2013) and Faure & Josselin (2008) lies in the replacement of $r_{0,j\rightarrow 0,j'}$ by $r_{1,j\rightarrow 0,j'}$. Although this change seems minor, the improvement in the estimated rate coefficients is substantial. We will show this in detail in Section 3, where we compare the extrapolated rates of $v = 2, j \rightarrow v' = 1, j'$ transitions with results obtained directly from CC calculations. The ro-vibrational rate coefficients $r_{1,j\rightarrow 0,j'}(T)$ have been calculated using the full CC method, while the vibrational rate coefficients $r_{v\rightarrow v'}(T)$ were obtained from the IOS approximation. All other ro-vibrational rate coefficients $r_{v,j\rightarrow v',j'}(T)$ can then be obtained from the extrapolation formula, Equation (5). Another advantage of our method is that it also yields the values for $v, j \rightarrow v', j' = j$ transitions; these could not be obtained with the previous extrapolation method since the data for rotationally elastic $j \rightarrow j$ transitions were not tabulated. And even if they had been available, they most likely would have given much too large extrapolated results.

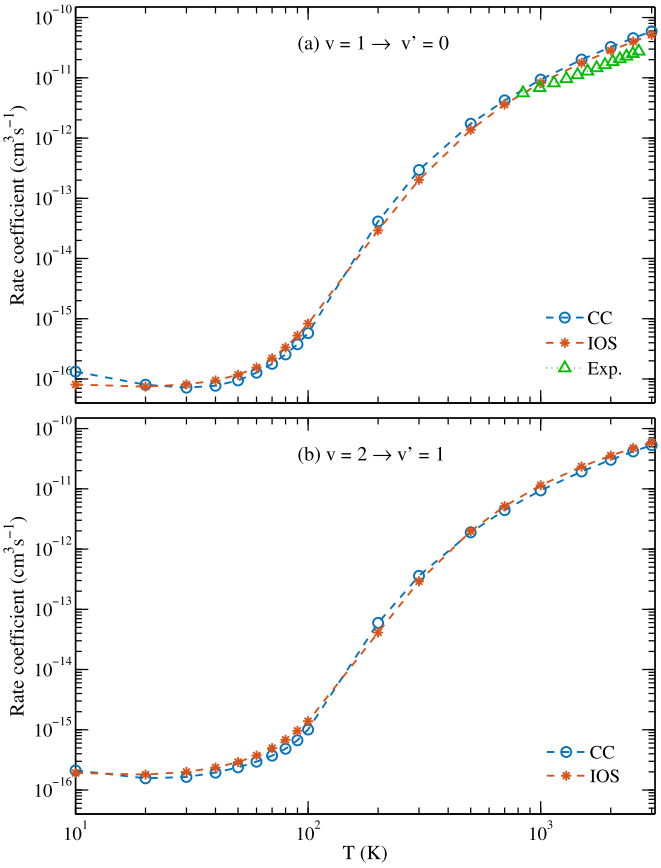

Figure 1. Comparison of CC and IOS rates for vibrational quenching $v = 1 \rightarrow v' = 0$ and $v = 2 \rightarrow v' = 1$. The experimental rates are from Glass & Kironde (1982).

3. RESULTS

3.1. Rate Coefficients from Quantum Scattering Calculations

Cross sections for ro-vibrational $v = 1, j = 0$–$30 \rightarrow v' = 0, j'$ transitions from full CC calculations are reported in our previous paper (Song et al. 2015). We also concluded in that paper that the coupled states approximation is only suitable for collision energies above $\approx$1000 cm^{-1} for the H–CO system and it is therefore not applied here. Table 1 lists the ro-vibrational transition rate coefficients for a gas temperature range of 10 K $\leqslant T \leqslant$ 3000 K calculated from these cross sections with the use of Equation (1). The highest final $j' = 27$ −42 values for which the rates are given in this table depend on the initial j quantum number. Transitions for even larger final j' are not reported, either because they are negligibly small, or because they were not completely converged with the largest number of partial waves, i.e., the highest total angular momentum J included. However, we add all final j' states, including those that may not be fully converged, to calculate the vibrational quenching cross sections $\sigma^{\rm CC}_{v,j\rightarrow v'}(E_k)$ and the vibrational transition rate coefficients $r^{\rm CC}_{v\rightarrow v'}(T)$. Hence, the CC vibrational quenching rate coefficients shown in Figure 1 are slightly different from the values that would be obtained by summing and averaging only the reported rates $r^{\rm CC}_{v,j\rightarrow v',j'}(T)$.

In order to test our proposed extrapolation scheme, we also calculated cross sections and rate coefficients for ro-vibrational $v = 2, j = 0$–$30 \rightarrow v' = 1, j'$ transitions with the CC method. We used a channel basis $B4(75, 65, 54, 41, 20)$, where the

Table 2

Rate Coefficients from CC Calculations for Ro-vibrational $v = 2, j = 0$–$30 \rightarrow v' = 1, j'$ Transitions in the Temperature Range of 10 K $\leqslant T \leqslant$ 3000 K (in Units of $cm^3\ s^{-1}$ with the Exponent Denoting Powers of 10)

		T (K)																		
j	j'	10	20	30	40	50	60	70	80	90	100	200	300	500	700	1000	1500	2000	2500	3000
0	0	3.814e-17	3.269e-17	3.445e-17	3.888e-17	4.467e-17	5.139e-17	5.892e-17	6.746e-17	7.789e-17	9.222e-17	1.654e-15	9.767e-15	5.489e-14	1.298e-13	2.628e-13	4.838e-13	6.837e-13	8.609e-13	1.016e-12
0	1	5.241e-17	3.537e-17	3.243e-17	3.475e-17	3.970e-17	4.645e-17	5.478e-17	6.516e-17	7.932e-17	1.011e-16	2.996e-15	1.754e-14	9.173e-14	2.081e-13	4.087e-13	7.353e-13	1.026e-12	1.283e-12	1.509e-12
0	2	7.974e-17	4.962e-17	3.823e-17	3.441e-17	3.412e-17	3.588e-17	3.920e-17	4.433e-17	5.256e-17	6.688e-17	2.499e-15	1.466e-14	6.790e-14	1.418e-13	2.623e-13	4.562e-13	6.375e-13	8.091e-13	9.696e-13

(This table is available in its entirety in machine-readable form.)

Table 3
CO Vibrational Energy Levels

v	ϵ_v(cm^{-1})	v	ϵ_v(cm^{-1})	v	ϵ_v(cm^{-1})
0	1082	5	11534	10	21331
1	3225	6	13546	11	23213
2	5342	7	15531	12	25069
3	7432	8	17490	13	26899
4	9496	9	19424	14	28704

notation $Bn(j_0, j_1, j_2, \ldots, j_n)$ represents a basis with the highest vibrational level n and the highest rotational level j_i for vibrational level $v = i$ (see Song et al. 2015). The state-to-state ro-vibrational rate coefficients were computed for a temperature range of 10 K $\leqslant T \leqslant$ 3000 K; they are listed in Table 2.

In addition, we obtained vibrational quenching cross sections from scattering calculations in the IOS approximation with a v = 0–14 basis for CO. This basis of 15 vibrational levels, with energies given in Table 3, is sufficiently large to converge all $v = 1$–$5 \rightarrow v' < v$ transitions. In Table 4 we report the IOS vibrational transition rate coefficients for a temperature range of 10 K $\leqslant T \leqslant$ 3000 K. The IOS approximation is not always suitable for cross sections at low collision energy and for rate coefficients at low temperature. We check this by comparing the vibrational rate coefficients produced with the IOS approximation and the results obtained by summing the state-to-state CC rate coefficients over final rotational j' levels and averaging over initial j levels. Figure 1 shows that the IOS rate coefficients agree well with the CC results, for both $v = 1 \rightarrow v' = 0$ and $v = 2 \rightarrow v' = 1$ transitions. The calculated results for the $v = 1 \rightarrow v' = 0$ transition also agree with the experimental data measured for this transition by Glass & Kironde (1982). All deviations between the IOS and CC rate coefficients in Figure 1 are less than 45%, which is sufficiently accurate for astrophysical applications. The IOS rate coefficients for $v = 4 \rightarrow v' = 1, 2, 3$ transitions in Table 4 at temperatures $T = 40$ and 50 K were obtained by interpolation of the rate coefficients at other temperatures. The original IOS data show a sharp peak around these temperatures due to resonance effects in the cross sections. However, the resonances in the IOS cross sections do not precisely coincide with the resonances in the cross sections from CC calculations (see Figure 2 of Song et al. 2015).

3.2. Extrapolated Rate Coefficients

First, we test the validity of the extrapolation method used by Thi et al. (2013) and Faure & Josselin (2008). Combining the IOS vibrational rate coefficient for the $v = 1 \rightarrow v' = 0$ transition with pure rotational (vibrationally elastic) rate coefficients from Walker et al. (2015), both of them based on the 3D H–CO potential of Song et al. (2013), we can obtain the state-to-state ro-vibrational rate coefficients for $v = 1, j = 0$–$30 \rightarrow v' = 0, j'$ transitions by extrapolation. Examples of the comparison of our CC rate coefficients, rate coefficients from extrapolation based on the method of Faure & Josselin (2008) and Thi et al. (2013), and the corresponding rate coefficients used by Thi et al. (2013) are illustrated in Figure 2. For transitions with final j' less than or close to the initial j, i.e., the $v = 1, j = 5 \rightarrow v' = 0, j' = 0, 6$ transitions, the CC and extrapolated rate coefficients agree quite well with each other, as shown in Figures 2(a) and (b). Large discrepancies appear, however, between CC and extrapolated rate coefficients for transitions with larger $\Delta j = j' - j$, especially at lower temperatures, see Figures 2(c) and (d). These large discrepancies result because the pure rotational (vibrationally elastic) transitions in $v = 0$ are endoergic for $j' > j$, while the ro-vibrational quenching processes $v = 1, j \rightarrow v' = 0, j'$ are exoergic for all $j' < 33$ even when $j = 0$. In addition, by analogy with Equation (6), the vibration-related scale factor $P_{vv'}(T)(v \neq v')$ can be rewritten in the extrapolation method of Thi et al. (2013) and Faure & Josselin (2008) as $r_{v\rightarrow v'}(T)/r_{0\rightarrow 0}(T)$. Clearly, the validity of scaling inelastic vibrational transition rate coefficients with vibrationally elastic data is questionable. The rate coefficients adopted in the modeling of Thi et al. (2013) are even more discrepant, as shown by the green lines with triangle markers in Figure 2. In their extrapolations, the pure rotational rates were adopted from Balakrishnan et al. (2002) who used the WKS potential, known to be inaccurate at long range. Moreover, the pure rotational rates for initial states with $j > 7$ and the vibrational rates for temperatures below 100 K were not available and had to be obtained by extrapolation.

Let us now discuss the results from our new extrapolation method based on vibrationally inelastic rates from quantum scattering calculations. Using the data in Tables 1 and 4, the ro-vibrational rate coefficients for $v = 2$–$5, j = 0$–$30 \rightarrow v' < v, j'$ transitions can be extrapolated with Equation (5). Figure 3 illustrates some comparisons of ro-vibrational rate coefficients for transitions from $v = 2, j$ to $v' = 1, j'$. It shows the full CC results, the rate coefficients from the new extrapolation method based on vibrationally inelastic data, and the results of Thi et al. (2013) based on vibrationally elastic data. For the four transitions shown, the new extrapolated rate coefficients agree very well with those from full CC calculations. The root mean square relative deviation of the rate coefficients in the temperature range of 10 K $\leqslant T \leqslant$ 3000 K for all the transitions $v = 2, j = 0$–$30 \rightarrow v' = 1, j'$ is 40%. This is sufficiently accurate for astronomical applications. However, the data from the scaling approach of Thi et al. (2013) deviate dramatically from our results, especially for higher final j' values. The reasons why their data are less accurate were already discussed above. The deviation is largest in the temperature range of 10 K $\leqslant T \leqslant$ 100 K, probably because the vibrational transition rate coefficients at low temperature were not available at the time.

4. ASTROPHYSICAL MODELS

In order to show the relevance of these new collision rate coefficients in the astrophysical context, we chose a twofold approach: (1) simple 1D slab models with constant temperature, density and CO abundance and (2) the 2D radiative thermo-chemical disk model from Thi et al. (2013). In the following, we compare the results obtained with the old H–CO collision rates to those obtained with the new data. Since this paper presents new collision rates for $v \leqslant 5$ and $j \leqslant 30$, we restricted the calculations below to the same range of quantum numbers.

4.1. ProDiMo Slab and Disk Models

ProDiMo is a 2D radiation thermo-chemical disk code (Woitke et al. 2009). The code solves the 2D continuum radiative transfer to obtain the dust temperature and radiation field throughout the disk and provides the self-consistent solution for the chemistry and gas heating/cooling balance.

Table 4

Rate Coefficients from IOS Calculations for Vibrational $v = 1$–$5 \rightarrow v' < v$ Transitions in the Temperature Range of $10\ \mathrm{K} \leqslant T \leqslant 3000\ \mathrm{K}$ (in Units of $\mathrm{cm}^3\ \mathrm{s}^{-1}$ with the Exponent Denoting Powers of 10)

		T (K)																		
v	v'	10	20	30	40	50	60	70	80	90	100	200	300	500	700	1000	1500	2000	2500	3000
1	0	8.076e-17	7.485e-17	8.113e-17	9.464e-17	1.172e-16	1.550e-16	2.205e-16	3.335e-16	5.233e-16	8.297e-16	2.929e-14	2.022e-13	1.372e-12	3.594e-12	8.206e-12	1.768e-11	2.833e-11	3.970e-11	5.148e-11
2	1	1.914e-16	1.808e-16	1.995e-16	2.355e-16	2.906e-16	3.728e-16	4.960e-16	6.817e-16	9.628e-16	1.388e-15	4.115e-14	2.911e-13	1.981e-12	5.144e-12	1.145e-11	2.339e-11	3.554e-11	4.746e-11	5.899e-11
2	0	1.164e-17	1.107e-17	1.284e-17	1.629e-17	2.189e-17	3.076e-17	4.478e-17	6.708e-17	1.028e-16	1.601e-16	7.337e-15	5.767e-14	4.257e-13	1.175e-12	2.858e-12	6.689e-12	1.141e-11	1.674e-11	2.243e-11
3	2	3.312e-16	3.008e-16	3.201e-16	3.648e-16	4.352e-16	5.387e-16	6.902e-16	9.164e-16	1.265e-15	1.819e-15	7.871e-14	5.598e-13	3.131e-12	7.056e-12	1.398e-11	2.613e-11	3.811e-11	4.963e-11	6.053e-11
3	1	3.662e-17	3.625e-17	4.124e-17	5.054e-17	6.567e-17	8.971e-17	1.279e-16	1.894e-16	2.891e-16	4.508e-16	1.987e-14	1.476e-13	1.016e-12	2.676e-12	6.112e-12	1.291e-11	2.005e-11	2.717e-11	3.406e-11
3	0	5.680e-18	5.697e-18	6.488e-18	7.930e-18	1.021e-17	1.372e-17	1.918e-17	2.772e-17	4.115e-17	6.197e-17	1.786e-15	1.396e-14	1.326e-13	4.246e-13	1.164e-12	3.023e-12	5.476e-12	8.346e-12	1.144e-11
4	3	4.033e-16	3.707e-16	4.219e-16	4.811e-16	5.567e-16	6.781e-16	8.705e-16	1.144e-15	1.536e-15	2.103e-15	5.222e-14	3.610e-13	2.252e-12	5.502e-12	1.169e-11	2.323e-11	3.498e-11	4.630e-11	5.674e-11
4	2	7.546e-17	7.361e-17	9.554e-17	1.142e-16	1.364e-16	1.774e-16	2.514e-16	3.682e-16	5.525e-16	8.418e-16	3.153e-14	2.262e-13	1.486e-12	3.758e-12	8.163e-12	1.624e-11	2.421e-11	3.179e-11	3.879e-11
4	1	2.871e-17	2.853e-17	3.229e-17	3.836e-17	4.831e-17	6.451e-17	9.013e-17	1.309e-16	1.956e-16	2.977e-16	1.101e-14	7.980e-14	5.566e-13	1.491e-12	3.481e-12	7.586e-12	1.209e-11	1.666e-11	2.107e-11
4	0	3.995e-18	4.021e-18	4.456e-18	5.319e-18	6.833e-18	8.506e-18	1.161e-17	1.648e-17	2.416e-17	3.621e-17	1.315e-15	9.893e-15	7.532e-14	2.202e-13	5.838e-13	1.543e-12	2.877e-12	4.477e-12	6.200e-12
5	4	5.545e-16	5.101e-16	5.345e-16	5.980e-16	7.035e-16	8.219e-16	1.011e-15	1.278e-15	1.663e-15	2.230e-15	5.837e-14	3.916e-13	2.265e-12	5.339e-12	1.116e-11	2.220e-11	3.355e-11	4.428e-11	5.376e-11
5	3	1.282e-16	1.278e-16	1.420e-16	1.690e-16	2.149e-16	2.637e-16	3.532e-16	4.925e-16	7.125e-16	1.063e-15	4.172e-14	2.906e-13	1.746e-12	4.176e-12	8.704e-12	1.692e-11	2.502e-11	3.254e-11	3.912e-11
5	2	7.653e-17	7.476e-17	8.187e-17	9.513e-17	1.153e-16	1.496e-16	2.000e-16	2.790e-16	4.050e-16	6.076e-16	2.524e-14	1.789e-13	1.100e-12	2.686e-12	5.718e-12	1.129e-11	1.677e-11	2.185e-11	2.632e-11
5	1	2.262e-17	2.159e-17	2.333e-17	2.676e-17	3.186e-17	4.143e-17	5.466e-17	7.517e-17	1.077e-16	1.603e-16	7.189e-15	5.332e-14	3.471e-13	8.958e-13	2.070e-12	4.606e-12	7.511e-12	1.049e-11	1.328e-11
5	0	2.629e-18	2.455e-18	2.621e-18	2.974e-18	3.497e-18	4.469e-18	5.769e-18	7.731e-18	1.079e-17	1.568e-17	7.253e-16	5.670e-15	4.002e-14	1.127e-13	2.974e-13	8.075e-13	1.548e-12	2.445e-12	3.394e-12

Notes. Rates for transitions for $v = 4 \rightarrow v' = 1$, 2, 3 at 40 and 50 K are obtained by spline interplation.

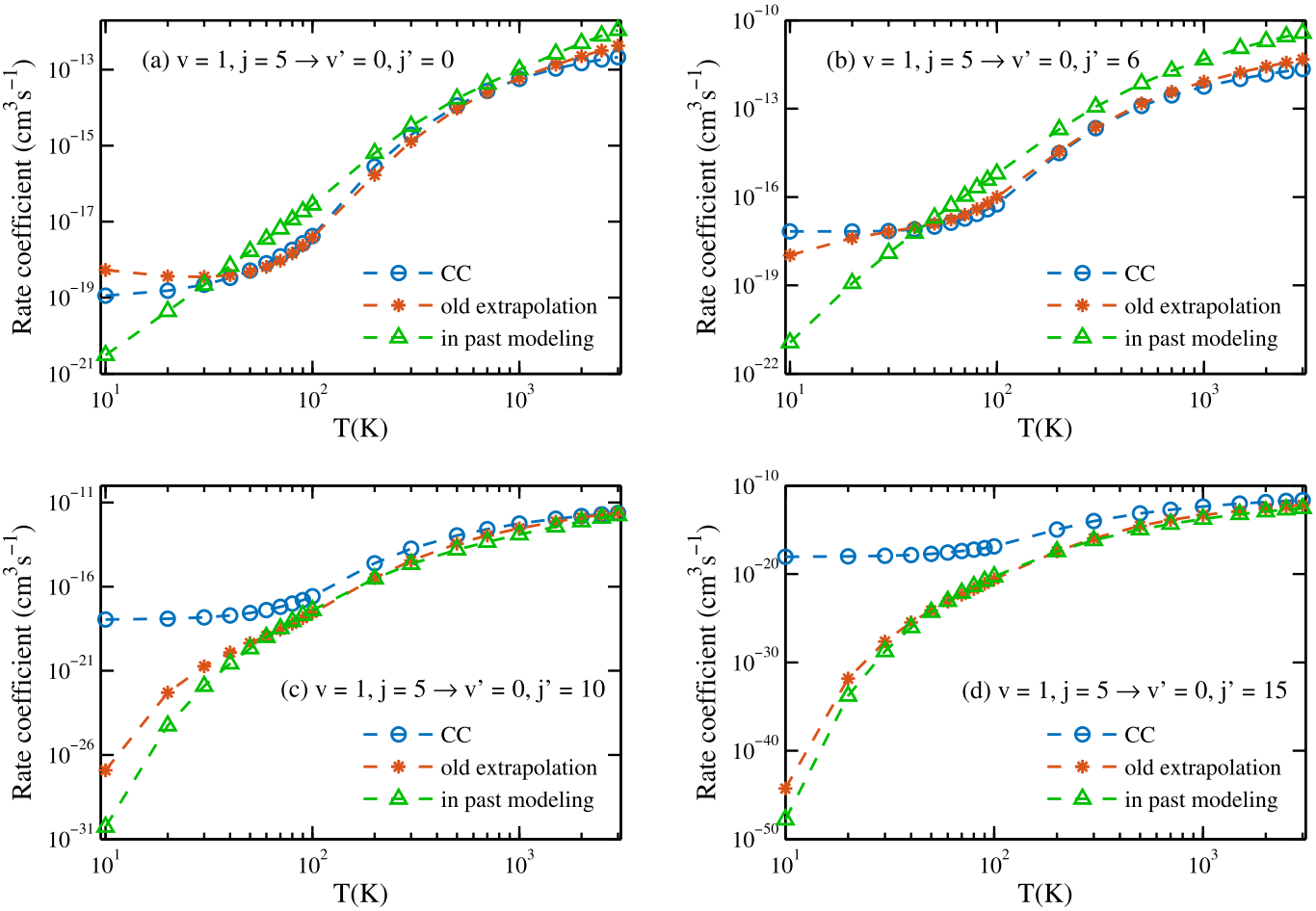

Figure 2. Comparison of ro-vibrational transition rate coefficients from CC calculations with extrapolated data obtained with the old extrapolation method of Thi et al. (2013) and Faure & Josselin (2008; using vibrationally elastic data) and with the data used in astrophysical modeling (Thi et al. 2013).

The gas temperatures can be used iteratively to find a vertical hydrostatic equilibrium solution. However, we use for this work a fixed parametrized gas scale height and assume that gas and dust are well mixed. Details of the numerical methods, the chemical network and a list of heating/cooling processes can be found in Woitke et al. (2009). The CO molecular data used are described in detail above and in Thi et al. (2013).

The code can be used in 1D slab mode, to calculate the emission emerging from a fixed total gas column with a constant gas temperature and constant volume densities of collision partners (H, H_2, He and e^-). The non-LTE level populations are calculated using the escape probability method taking into account also IR pumping by thermal dust emission. Since we focus here on the effect of the new collisional rates, we minimize the effect of IR pumping by fixing the dust temperature at 20 K. The turbulent width is fixed to $v_{\rm turb} = 1.0$ km s^{-1} and the total broadening is given by $b = \sqrt{v_{\rm th}^2 + v_{\rm turb}^2}$, where $v_{\rm th}$ is the thermal velocity of the CO molecules. The slab models provide a powerful means to exploit a very wide parameter space under which CO emission could arise in space.

In addition, we use the standard model for a disk around a 2.2 $M_\odot$ Herbig star ($L_* = 32 L_\odot$) taken from Thi et al. (2013). The disk has a radial size of 300 AU and a mass of $10^{-2} M_\odot$. More details on the dust opacities and vertical disk structure can be found in Table 3 of Thi et al. (2013). Such a disk model does not provide any freedom as to the conditions under which CO is emitting. Its abundance, excitation and emission are calculated self-consistently given the density distribution of gas within the disk and the irradiating stellar and interstellar radiation field.

4.2. Slab Model Results

We ran four series of models, each with three different total gas column densities of $N_{\langle \rm H \rangle} = 10^{19}$, 10^{21}, and 10^{23} cm^{-2}. The CO abundance is fixed at 10^{-4} with respect to the total hydrogen number density. Series 1 uses a fixed gas temperature T of 800 K and high densities of collision partners, $\log n_{\rm H} = \log n_{\rm H_2} = 9$, $\log n_{\rm He} = 8$, $\log n_{\rm e} = 5$ (in cm^{-3}). Note that the gas in these slab models is not fully molecular, i.e., the H/H_2 abundance ratio is 1. Series 2 uses a lower gas temperature of 200 K and the same collision partner densities. Series 3 uses $T = 800$ K and a lower density of collision partners, $\log n_{\rm H} = \log n_{\rm H_2} = 6$, $\log n_{\rm He} = 5$, $\log n_{\rm e} = 2$ (in cm^{-3}). An additional series (4) was calculated to isolate the effect of H-collisions. In this series, the temperature and density of H are the same as in series 3, while the collision partner densities of H_2, He and electrons are assumed to be negligible.

Figure 4 illustrates the change in the non-LTE fluxes of the $v = 1-0$ band resulting from the old and new collisional rates for H–CO in the slab models. We note that changes are typically smallest for the slab with the largest line optical depth $\log N_{\langle \rm H \rangle} = 23$ ($\log N_{\rm CO} = 19$). For slabs at $T = 800$ K, the line

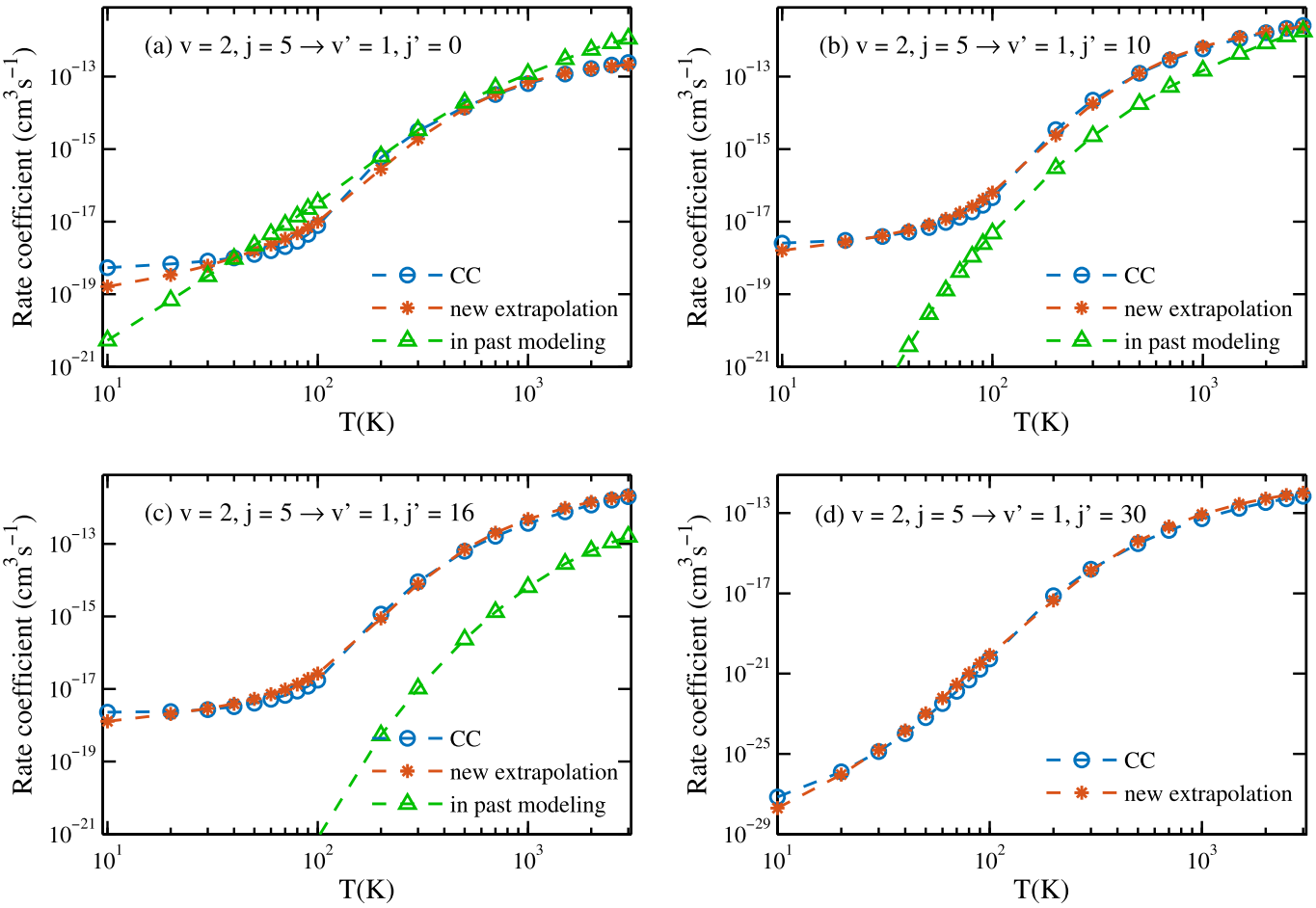

Figure 3. Comparison of ro-vibrational transition rate coefficients from CC calculations with extrapolated data obtained with our new extrapolation method (using vibrationally inelastic data) and with the data used in astrophysical modeling (Thi et al. 2013).

fluxes with the new rates are smaller than those with the old rates. Exceptions are the smaller and the highest j levels; the flux changes are generally largest for the lowest four levels. It is also evident from these comparisons that the implementation of the new rates will have an effect on the shape of the vibrational band structure. In most cases of high T (800 K) slabs, the band structure (flux versus wavelength) will get flatter for low j and drop faster at high j compared to the band structure with the old collision data. The total cooling rate of the $v = 1-0$ band ($j \leqslant 30$) is typically 20%–30% lower with the new collisional rates. This will have an impact on the gas temperature whenever CO cooling dominates the energy balance. Examples are (1) the surface layers of the inner $\approx$10 pc of active galactic nucleus (AGN) disks (Meijerink et al. 2013), (2) the inner $\approx$10 AU of protoplanetary disks (Woitke et al. 2009) and (3) intermediate density ($n_{\langle H \rangle} \approx 10^5$ cm^{-3}) J-type shocks (Hollenbach & McKee 1989). If H collisions are omitted entirely in slab series 1, the fluxes in the most optically thick case are lower by a factor of 100; hence H collisions are more important than H_2 collisions and they are key in modeling the CO ro-vibrational emission.

The gas temperature T is a free parameter and we can explore the effect of the new collision rates at lower temperatures. The comparison between series 1 and 2 (top left and right panel of Figure 4) clearly shows that the changes in the line fluxes increase substantially for $T = 200$ K. However, at these low temperatures, the populations in the CO vibrational levels are very low and hence also the emerging line fluxes will be low. An exception may be the case of fluorescent excitation, where the vibrational levels are populated by an external radiation field to non-LTE values. Examples are the inner disks of Herbig Ae stars, where the stellar radiation field can substantially pump the vibrational levels to vibrational temperatures of a few thousand K (Brittain et al. 2009; van der Plas et al. 2015).

The bottom panels of Figure 4 illustrate the effects for low density environments (non-LTE cases). Here, line-to-line differences are larger than in the high density environment. The overall picture does not change very much if we neglect the other collision partners, H_2, He, and electrons.

Besides the application to protoplanetary disks discussed in the next section, these new rate coefficients will also be important for proper modeling of CO infrared emission from other interstellar regions with large H/H_2 transition zones such as dissociative J-type shocks (Neufeld & Dalgarno 1989; González-Alfonso et al. 2002) or dense X-ray irradiated gas found near AGNs.

4.3. Disk Model Results

Figure 5 shows the change in the CO ro-vibrational emission of the $v = 1-0$ band at 4.7 μm resulting from the old and the new (this work) H–CO collision rate coefficients. The collision rate coefficients with H_2, He, and electrons remain unchanged.

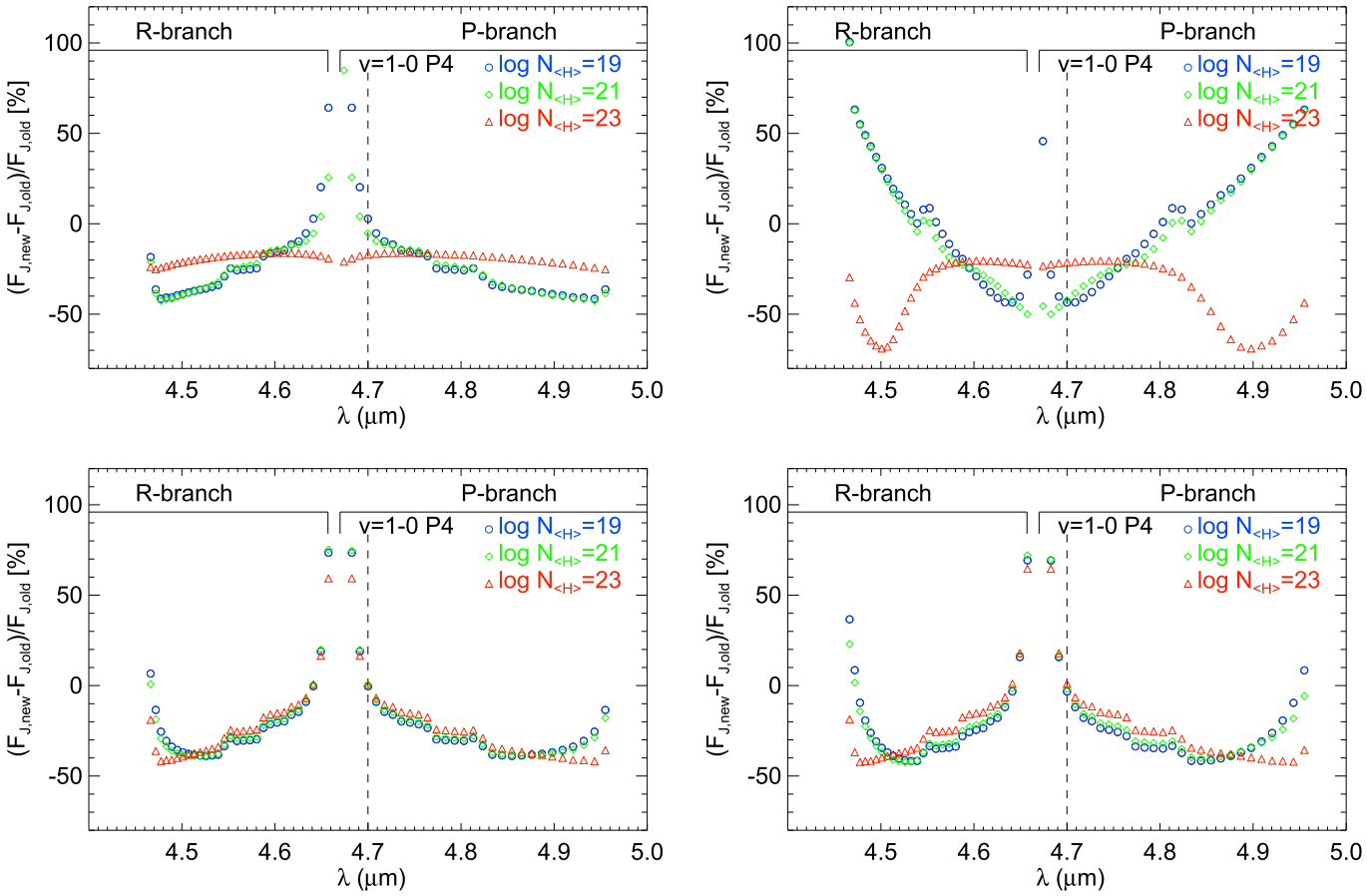

Figure 4. Changes in the modeled CO ro-vibrational emission from a series of slab models using the new and previously available H–CO rate coefficients. Top left (series 1): $T = 800$ K, $\log n_{\rm H,H_2} = 9$, $\log n_{\rm He} = 8$, $\log n_{\rm e} = 5$ in units of cm^{-3}. Top right (series 2): $T = 200$ K, $\log n_{\rm H,H_2} = 9$, $\log n_{\rm He} = 8$, $\log n_{\rm e} = 5$. Bottom left (series 3): $T = 800$ K, $\log n_{\rm H,H_2} = 6$, $\log n_{\rm He} = 5$, $\log n_{\rm e} = 2$. Bottom right (series 4): $T = 800$ K, $\log n_{\rm H} = 6$, collisions with other partners negligible. The total gas column density of the slab $N_{\langle \rm H \rangle}$ is given in the legend.

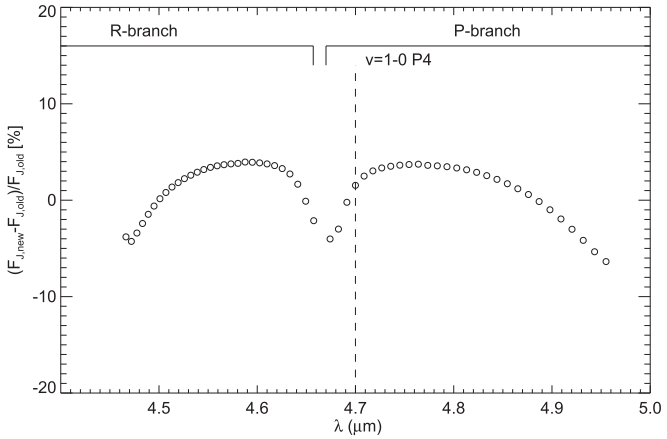

Figure 5. Changes in the modeled CO ro-vibrational emission from the disk around a Herbig Ae star using the new and previously available H–CO rate coefficients.

Differences are small, on the order of ±5%. The line fluxes with the new rates show a clear pattern with respect to the old ones: the new rates lead to lower line fluxes at low j, higher fluxes in the intermediate range and then again lower fluxes for $j \gtrsim 25$. The upturn at the highest j is a boundary effect, since the rotational states of CO are artificially cut off in the model at $j = 30$. As noted in Thi et al. (2013), the CO emission arises from a hot surface layer with $T \approx 1000$ K, where the gas is predominantly atomic (see their Figure 12). At these high temperatures, differences between the old and new collision rates are smaller than at low temperatures (Figure 2) and this partially explains the relatively small changes observed in the disk model. In addition, IR pumping is competing with collisions, especially in the inner disk, where dust continuum emission peaks in the near-IR (1000 K $< T_{\rm dust} <$ 1500 K).

5. CONCLUSIONS

We present ro-vibrational de-excitation rate coefficients from full CC quantum scattering calculations for $v = 1, j =$ 0–30 $\rightarrow v' = 0, j'$ and $v = 2, j =$ 0–30 $\rightarrow v' = 1, j'$ transitions of CO in collision with H atoms in the temperature range of 10 K $\leqslant T \leqslant$ 3000 K. Also vibrational quenching rate coefficients from IOS calculations are given for $v =$ 1–5 $\rightarrow v' < v$ transitions in the same temperature range. We propose a new extrapolation method to obtain the ro-vibrational rate coefficients for $v =$ 2–5, $j =$ 0–30 $\rightarrow v' < v, j'$ transitions from our quantum mechanically calculated results. Comparison of the CC ro-vibrational rate coefficients for the $v = 2, j =$ 0–30 $\rightarrow v' = 1, j'$ transitions with the extrapolated ones confirms the reliability of this extrapolation method. A LAMDA-type (Schöier et al. 2005) file with state-to-state ro-vibrational rate coefficients for $v =$ 1–5, $j =$ 0–30 $\rightarrow v' < v, j'$ transitions is provided online. Compared with the ro-vibrational

rate coefficients for H–CO used previously in astrophysical modeling (Thi et al. 2013), the current data set is both comprehensive and accurate. The application of the previously available and the new data set in slab models shows that typical changes in line fluxes under astrophysical conditions are on the order of 20%–70% in high temperature environments (800 K) with an H/H_2 ratio of 1 and increase for lower temperatures. In the inner disks around Herbig Ae stars, the line flux changes are smaller due to the very high temperatures and densities under which this emission arises.

We are grateful to Ewine van Dishoeck for suggesting this study and we thank her, Simon Bruderer, and François Lique for valuable discussions. We thank the computer and communication department (C&CZ) of the Faculty of Science of the Radboud University for computer resources and technical support. The work is supported by The Netherlands Organisation for Scientific Research, NWO, through the Dutch Astrochemistry Network, and in part by the National Science Foundation under grant No. NSF PHY11-25915. N.B. is supported in part by NSF grant PHY-1505557. K.M.W. and P.C.S. acknowledge support from NASA grants NNX12AF42G and NNX13AF42G. I.K. and W.F.T. acknowledge funding from the European Union Seventh Framework Programme FP7-2011 under grant agreement no. 284405.

REFERENCES

Ayres, T. 1986, HiA, 7, 425
Balakrishnan, N., Yan, M., & Dalgarno, A. 2002, ApJ, 568, 443
Bertelsen, R., Kamp, I., Goto, M., et al. 2014, A&A, 561, A102
Brittain, S. D., Najita, J. R., & Carr, J. S. 2009, A&A, 702, 85
Brown, J. M., Pontoppidan, K. M., van Dishoeck, E. F., et al. 2013, ApJ, 770, 94
Bruderer, S., Harsono, D., & van Dishoeck, E. F. 2015, A&A, 575, A94
Carmona, A., van den Ancker, M. E., Thi, W.-F., Goto, M., & Henning, T. 2005, A&A, 436, 977
Chu, S.-I., & Dalgarno, A. 1975, RSPSA, 342, 191
Faure, A., & Josselin, E. 2008, A&A, 492, 257
Glass, G. P., & Kironde, S. 1982, JPhCh, 86, 908
González-Alfonso, E., Wright, C. M., Cernicharo, J., et al. 2002, A&A, 386, 1074
Goto, M., Regály, Zs., Dullemond, C. P., et al. 2011, ApJ, 728, 1
Green, S., & Thaddeus, P. 1976, ApJ, 205, 766
Hollenbach, D., & McKee, C. F. 1989, ApJ, 342, 306
Hutson, J. M., & Green, S. 1994, Molscat computer code, version 14 (1994), distributed by Collaborative Computational Project No. 6 of the Engineering and Physical Sciences Research Council (UK)
Johnson, H. L., & Méndez, M. E. 1970, AJ, 75, 785
Johnson, H. L., Thompson, R. I., Forbes, F. F., & Steinmetz, D. L. 1972, PASP, 84, 775
Keller, H.-M., Floethmann, H., Dobbyn, A. J., et al. 1996, JChPh, 105, 4983
Kozlov, P., Makarov, V., Pavlov, V., & Shatalov, O. 2000, ShWav, 10, 191
Meijerink, R., Spaans, M., Kamp, I., et al. 2013, JPCA, 117, 9593
Mitchell, G. F., Maillard, J.-P., Allen, M., Beer, R., & Belcourt, K. 1990, ApJ, 363, 554
Najita, J., Carr, J. S., & Mathieu, R. D. 2003, ApJ, 589, 931
Neufeld, D. A., & Dalgarno, A. 1989, ApJ, 340, 869
Pontoppidan, K. M., Blake, G. A., van Dishoeck, E. F., et al. 2008, ApJ, 684, 1323
Rettig, T. W., Haywood, J., Simon, T., Brittain, S. D., & Gibb, E. 2004, ApJL, 616, L163
Salyk, C., Blake, G. A., Boogert, A. C. A., & Brown, J. M. 2007, ApJL, 655, L105
Schöier, F. L., van der Tak, F. F. S., van Dishoeck, E. F., & Black, J. H. 2005, A&A, 432, 369
Scoville, N. Z., Krotkov, R., & Wang, D. 1980, ApJ, 240, 929
Shepler, B. C., Yang, B. H., Dhilip Kumar, T. J., et al. 2007, A&A, 475, L15
Song, L., Balakrishnan, N., van der Avoird, A., Karman, T., & Groenenboom, G. C. 2015, JChPh, 142, 204303
Song, L., van der Avoird, A., & Groenenboom, G. C. 2013, JPCA, 117, 7571
Thi, W. F., Kamp, I., Woitke, P., et al. 2013, A&A, 551, A49
Thompson, R. I., Schnopper, H. W., Mitchell, R. I., & Johnson, H. L. 1969, ApJL, 158, L117
van der Plas, G., van den Ancker, M. E., Acke, B., et al. 2009, A&A, 500, 1137
van der Plas, G., van den Ancker, M. E., Waters, L. B. F. M., & Dominik, C. 2015, A&A, 574, A75
van der Tak, F. 2011, in IAU Symp. 280, The Molecular Universe, ed. J. Cernicharo & R. Bachiller (Cambridge: Cambridge Univ. Press), 449
von Rosenberg, C. W., Taylor, R. L., & Teare, J. D. 1971, JChPh, 54, 1974
Walker, K. M., Song, L., Yang, B. H., et al. 2015, ApJ, 881, 27
Walker, K. M., Yang, B. H., Stancil, P. C., Balakrishnan, N., & Forrey, R. C. 2014, ApJ, 790, 96
Woitke, P., Kamp, I., & Thi, W.-F. 2009, A&A, 501, 383
Yang, B., Stancil, P. C., & Balakrishnan, N. 2005, JChPh, 123, 094308
Yang, B., Stancil, P. C., Balakrishnan, N., Forrey, R. C., & Bowman, J. M. 2013, ApJ, 771, 49